Information Sciences 181 (2011) 2797–2812

Contents lists available at ScienceDirect

Information Sciences

journal homepage: www.elsevier.com/locate/ins

Artificial immune multi-objective SAR image segmentation with fused complementary features

Dongdong Yang *, Licheng Jiao, Maoguo Gong, Fang Liu

Key Lab of Intelligent Perception and Image Understanding of Ministry of Education of China, Institute of Intelligent Information Processing, Xidian University, Xi'an 710071, China

ARTICLE INFO

Article history:
Received 14 January 2010
Received in revised form 21 February 2011
Accepted 26 February 2011
Available online 5 March 2011

Keywords:
Evolutionary computation
Artificial immune system
Single-objective optimization (SO)
Multi-objective optimization (MO)
Clustering validity indices
Feature fusion
Gabor filter
Gray level co-occurrence probability

ABSTRACT

Artificial immune systems (AIS) are the computational systems inspired by the principles and processes of the vertebrate immune system. AIS-based algorithms typically mimic the human immune system's characteristics of learning and adaptability to solve some complicated problems. Here, an artificial immune multi-objective optimization framework is formulated and applied to synthetic aperture radar (SAR) image segmentation. The important innovations of the framework are listed as follows: (1) an efficient and robust immune, multi-objective optimization algorithm is proposed, which has the features of adaptive rank clones and diversity maintenance by *K*-nearest-neighbor list; (2) besides, two conflicting, fuzzy clustering validity indices are incorporated into this framework and optimized simultaneously and (3) moreover, an effective, fused feature set for texture representation and discrimination is constructed and researched, which utilizes both the Gabor filter's ability to precisely extract texture features in low- and mid-frequency components and the gray level co-occurrence probability's (GLCP) ability to measure information in high-frequency. Two experiments with synthetic texture images and SAR images are implemented to evaluate the performance of the proposed framework in comparison with other five clustering algorithms: fuzzy *C*-means (FCM), single-objective genetic algorithm (SOGA), self-organizing map (SOM), wavelet-domain hidden Markov models (HMTseg), and spectral clustering ensemble (SCE). Experimental results show the proposed framework has obtained the better performance in segmenting SAR images than other five algorithms and behaves insensitive to the speckle noise.

1. Introduction

Synthetic aperture radar (SAR) is a kind of active microwave instrument, producing high-resolution imagery of the Earth's surface in all weather. It has been widely utilized in environmental monitoring, earth-resource mapping and military systems. An important issue in the SAR image applications is the correct segmentation and identification of objectives in them, which is essential to understand the image clearly. The major purpose of image segmentation is to partition an image into regions of different characteristics such that the pixels in the same group are more similar to each other than pixels in different groups. The difficulties existing in SAR image segmentation are the highly overlapped pixels and large amounts of unpredictable and inestimable speckle noise in this kind of image. The existence of noise deteriorates the quality of SAR images seriously and can conceal important details, leading to the loss of interesting objectives. To date, many SAR image

* Corresponding author. Address: Mail Box 224, Xidian University, No. 2 South TaiBai Road, Xi'an 710071, China.
E-mail addresses: xuridongsheng150@163.com, ddyang@mail.xidian.edu.cn (D. Yang).

0020-0255/$ - see front matter © 2011 Elsevier Inc. All rights reserved.
doi:10.1016/j.ins.2011.02.025

segmentation methods have been proposed and studied, including clustering-based methods [29,35,60], graph-partitioning methods [33], morphologic methods [34], and model-based methods [20,53].

Evolutionary computation (EC) uses the computational models of the human evolution as key elements in the design and implementation of computer-based problem-solving systems. It has become an important part of artificial intelligence. Many EC computing paradigms have been proposed and applied to real-world problems during the last two decades [47], such as genetic algorithm [52,26], particle swarm optimization [5], genetic programming [3], and artificial immune system (AIS) [16,23]. AIS, focusing on improve the computation efficiency of traditional genetic algorithm, attempts to extract the features of learning, memory and adaptability from biological immune systems to develop computational tools for dealing with science and engineering problems. Recently, AIS-based algorithms have begun to emerge as problem solvers in image segmentation and pattern classification [2,44,54]. The current AIS algorithms can be divided into two categories: the single-objective algorithms and multi-objective ones. The single-objective algorithms of image classification are reviewed shortly as follows. An early paper introduced the use of the negative selection mechanism of the immune system in the literature [14] to detect anomalies in time series data. After that, McCoy and Devarajan [38] were the first paper to employ the negative selection algorithm in AIS to construct a set of class detectors in remotely sensed image segmentation. Besides, Timmis and de Castro are the two famous pathfinders, who have devoted themselves to the theoretical foundation of AIS algorithms [15,43]. With the increasing maturity of AIS theory, the applications of AIS into image processing have been quickly developed in recent years. In the paper [27], an immune kernel clustering network by combining of artificial immune network and description in support vector domain for unsupervised SAR image segmentation was proposed. Zhong et al. [59] presented a multi-valued immune network for supervised, remote-sensing image classification in another paper. However, due to the inherent complexity of artificial immune networks, their application to image classification is rather limited. In contrast, clonal selection algorithms have been widely applied to pattern recognition and image processing for their efficiency and simplicity. Zhang et al. [57] presented three novel dimensionality reduction methods by clonal selection theory for hyperspectral imagery segmentation. Zheng et al. [58] employed clonal selection algorithm to detect texture objects in satellite images. The artificial immune approach is utilized to automatically generate segmentation thresholds by using the roughness of texture objects. In another paper by Zhang [56], he provided a new feature selection approach that uses clonal selection algorithm for SAR image classification. The texture feature set for the SAR image was formed by three feature extraction methods: the gray-level co-occurrence matrix, the gray-gradient co-occurrence matrix, and the energy measures of the undecimated wavelet decomposition. To date, most of above classification techniques employed only one objective function to assess the goodness of the quality of partitions. The objective function is assumed to reflect the quality of the partitions. This assumption may be very appropriate for particular type of data sets, but it cannot discover complicated and diverse characteristics for other types of data sets. Hence, it is necessary to consider multiple clustering objectives and optimize them simultaneously, especially for the data sets with different characteristics of shapes. Recently, AIS-based multi-objective algorithms have attracted a large amount of interests. Yet, the applications of them to image classification are seldom involved. In our previous works, we have presented two distinguished AIS-based multi-objective algorithms [48,49] and attempt to apply them into image classification [50].

In this paragraph, some typical AIS-based multi-objective algorithms and their characteristics are discussed. Many AIS-based multi-objective optimization algorithms have been proposed since the first pioneering study on EMO emerged in 1984 [41]. Coello has provided a general overview of the work in the last 20 years in EMO [11]. The pioneering work using AIS in EMO was detailed in Yoo and Hajela's article [51]. Afterwards, Cutello et al. [13] proposed a modified version of Pareto archived evolution strategy algorithms (I-PAES) using the notion of polypeptide chain and two immune inspired operators: cloning and hypermutation. Then, Coello and Cortés formally firstly employed clonal selection principal to present a famous multi-objective optimization algorithm in [12]. In another paper [36], Luh and Chueh simulated the antibody-antigen relationship in terms of specificity, germinal center, and the memory characteristics of adaptive immune responses to devise an efficient multi-objective immune algorithm. In the paper by Freschi and Repetto [21], they introduced the vector artificial immune system to multi-objective optimization. Their algorithm adopted random and uniform initialization, fixed-number clonal, negative exponent mutation, and diversity maintenance through a novel suppression operator. Significantly, Gong et al. [22] proposed a multi-objective, immune algorithm with non-dominated, neighbor-based selection (NNIA), including the novel strategies of non-dominated, neighbor-based selection strategy, crowding-distance based proportional cloning, simulated binary crossover, and a static hypermutation operator. The comparison and analysis showed that NNIA is an effective immune inspired, multi-objective algorithm. However, this algorithm may be trapped in a local optimal front if there are few non-dominated antibodies for online proportional cloning. Besides, it has been shown that the one-off deletion technique by crowding-distance in NNIA cannot estimate crowdedness well for diversity maintenance [32]. Hence, the robustness, diversity holding technique, and adaptability of NNIA can be further improved. Here, an enhanced version of NNIA is presented and applied to SAR imagery segmentation.

In this paper, we present an effective immune, multi-objective framework for SAR image segmentation (called IMIS for short). The simultaneous optimization of multiple-objectives is different from single-objective optimization in that there is no unique optimal solution to multi-objective problems. Multi-objective optimization usually involves many conflicting, incomparable, and non-commensurable objectives; therefore, a set of optimal tradeoff solutions known as the Pareto-optimal solutions can be obtained. The optimal or user wanted partitions of the image data can be selected from the tradeoff Pareto-optimal solutions. The novelty of IMIS lies in the following issues: (1) an effective, immune, multi-objective, SAR image segmentation method is proposed, which has the strategies of adaptive rank clones and diversity maintaining by

K-nearest-neighbor list; (2) two conflicting, fuzzy clustering validity indices are incorporated into the method and simultaneously optimized. The searching process regulated by the two indices can set foot more wider feasible regions, which is beneficial to identify promising solutions; (3) in order to obtain sufficient information for SAR image feature representation and discrimination, we constructed a fused feature set both by Gabor filter [30] and GLCP [25], which can be provided with complementarily advantageous for bandwidth responses in different frequency. Finally, we compared the method with five classification algorithms in segmenting the synthetic texture and SAR images to validate the performance of the proposed methodology. The experimental results show that encouraging and impressive performance in partitioning the five images are obtained by IMIS. Additionally, we also investigated the sensitivity of the introduced parameters and the robustness of IMIS to different levels of noise.

The remainder of the study is organized in the following way. Section 2 presents the basic definitions of immune, multi-objective optimization. Section 3 describes the details of the feature extraction techniques and the AIS-based, multi-objective, SAR segmentation framework. Next, the experimental validation and results analysis are shown. Finally, we outline the conclusion of the paper.

2. Definitions of AIS-based, multi-objective optimization

In this study, the following type of multi-objective optimization is considered [17].

$$Min \quad F(x) = (f_1(x), f_2(x), \ldots, f_K(x))^T \tag{1}$$

subject to $x \in \Omega$. Where $\boldsymbol{x}$ is a decision variable vector and Ω is the search space. $F : x \to R^K$ is the map of decision variable space to the space of K objectives. The objectives in multi-objective optimization usually conflict with each other and no single solution can optimize all the objectives simultaneously. In this framework, two conflicting and complementary indices, called XB [46] and JM [37], are used as two of the optimization objectives, which can be defined as follows:

$$\begin{aligned} \mathrm{XB} &= \frac{\sum_{p=1}^{k}\sum_{i,j=1}^{N} u_{pj}^2 \|x_j - z_p\|^2}{N \min\limits_{i,j} \|z_i - z_j\|}, \\ J_m &= \sum_{j=1}^{N}\sum_{p=1}^{k} u_{pj}^2 \|x_j - z_p\|^2, \end{aligned} \quad \text{where } u_{pj} = 1 \Big/ \sum_{i=1}^{k} \left(\frac{\|z_p - x_j\|}{\|z_p - x_i\|} \right)^2 \tag{2}$$

Note that x_i, $i = 1, 2, \ldots, N$ is a data sample in a clustering data set and z_p, $p = 1, 2, \ldots, k$ is the cluster center. N is the total number of samples and k is the number of categories. $U_{k\times N}$ is the fuzzy membership matrix. XB is formulated by the ratio of the summation of variation to the minimum separation. The lower values of XB could provide a better partition of the data set. JM is defined by minimizing the global, fuzzy squared distance. Bandyopadhyay et al. [1] have noted that the two indices revealed contradictory characteristics and can provide a rich set of alternate partitions for the remote sensing data. Significantly, a desirable searching process should guide the population from multiple directions since we have no prior knowledge about the optimal solution locations. Here, two conflicting indexes can guide the population into more spread feasible area than the traditional manners with only one index. Thus, multi-objective optimization algorithms can find the optimal partition with the larger probability than the single-objective optimization algorithms.

The domain knowledge is often utilized to select the final optimal solution in multi-objective optimization because there is no explicit and general methodology to classify images in all styles. However, sometimes such a priori knowledge might not be available for complicated and tight classification tasks. Hence, a tradeoff index (called PBM) is employed for the final optimal solution selection. This index has demonstrated superior performance to three other frequently used indices paper [37]. The definition of the index could be described in the following way:

$$PBM(k) = \left(\frac{1}{k} \times \frac{E_1}{E_k} \times D_k \right)^2, \text{ where } E_k = \sum_{p=1}^{k}\sum_{j=1}^{N} u_{pj}\|x_j - z_p\| \text{ and } D_k = \max_{i,j=1}^{k} \|z_i - z_j\| \tag{3}$$

The definitions of the symbols: x_j, z_p, u_{pj} in (3) are same in Eq. (2). The PBM index consists of three items: k, E_k, and D_k. k is the number of clustering, E_k is the total variations of a partition, and D_k is used to measure the maximum separation among clusters. These three factors are designed to compete with each other to achieve proper partitioning. The maximization of PBM index could lead to a partition with the benefit of the least number of compact clusters and a large separation between at least two clusters.

Some notations in AIS-based multi-objective optimization are presented in this paragraph. An antigen in AIS is usually defined as a searching problem [15]. Here, the MOPs defined by Eq. (1) can be seen as the antigen of multi-objective optimization. The candidate solutions of Eq. (1) are named antibodies in the immune system. The binding intensity between antigen and antibody is called the antigen-antibody affinity, which are the values of objective functions in Eq. (2). The candidate solutions are called antibodies and their objective values are called the affinity in following sections because an immune inspired algorithm is discussed here.

The concept of dominance in MO is described here. An antibody $u = (u_1, u_2, \ldots, u_K)$ is said to dominate another antibody $v = (v_1, v_2, \ldots, v_K)$ (denoted by $\boldsymbol{u} \prec \boldsymbol{v}$) if and only if $\boldsymbol{u}$ is partially less than $\boldsymbol{v}$, which can be defined by the following expression:

$$\forall i \in \{1, \ldots, K\}, \quad u_i \leqslant v_i \wedge \exists j \in \{1, \ldots, K\} : u_j < v_j \tag{4}$$

where ^ is a logic symbol, which means two concurrent terms. Furthermore, we say that an antibody $x^* \in \Omega$ is Pareto-optimal or a non-dominated solution in the problem (1) if another antibody, $x \in \Omega$ does not exist such that $x \prec x^*$. All the non-dominated antibodies in the decision space are made up of antibodies of the best rank. Once the non-dominated antibodies are removed from the current population, the non-dominated antibodies among the remaining population are called the next-best-rank antibodies. Through the operator of repetition, all the antibodies in the population can be assigned to be at different ranks. The rank-based adaptive selection and clones are the main characteristics of the proposed AIS-based, multi-objective, segmentation algorithm, which will be discussed in subsequent section.

3. An immune, multi-objective framework for SAR image segmentation

3.1. The stage of features extraction and preprocessing

In this study, the process of SAR image segmentation is divided into two stages. As shown in Fig. 1, the first stage is characterized by initially segmenting the SAR image and extracting features. Evolutionary computation with population iteration on the level of pixels is usually very time consuming because the number of pixels in a SAR image is very high, even for small images of moderate resolution. Therefore, a preprocessing stage is required to over-segment the original image into non-overlapping small patches or "superpixels". Additionally, proper features extraction techniques are necessary to differentiate the land covers in SAR images accurately. Here, two complementary feature extraction methods are employed and combined for image presentation and discrimination. Afterwards, the fused features are mapped by the over-segmented results of original image so as to obtain the over-segmented extracted image features. In other words, if the pixels are in the same patch in the over-segmented image, their features are classified into the same group correspondingly. In the second stage, an AIS-based multi-objective algorithm is proposed and a fine classification on the over-segmented results is carried out by the algorithm. The preprocessing techniques in the first stage are discussed as follows.

3.1.1. Watershed raw segmentation

The well-known watershed transformation [45] is used to partition an image into non-overlapping and homogeneous regions. The definition of the watershed transformation is in the following equation:

$$WT(I) = \frac{1}{N}\sum_{i=1}^{N}[I \oplus B_i - (I \ominus B_i) \ominus B_{i-1}] \tag{5}$$

where $\oplus$ and $\ominus$ denote dilation and erosion operations in mathematical morphology, respectively. B_i is called the structural window with size of $(2i-1)\times(2i-1)$, and I is the original image. It is far from an easy task to extract suitable watersheds on SAR images. If the watershed regions are too large, it may contain more than one objects of interest in the same basin; on the contrary, only one objective may not be in the same local patch and the available algorithms for computing the watershed transformation may be excessively slow. In this study, the dilation and erosion operations are both on a 3×3 window and about 1000 small pathces are obtained in the image with 256×256.

3.1.2. Feature extraction using Gabor filters and GLCP

Texture is an important characteristic for identifying objects or regions of interest in an image. To date, a large number of techniques for analyzing image texture have been proposed throughout the last three decades. Popular methodologies can be divided into three categories: statistical methods, model-based methods, and signal processing techniques. Markov random fields (MRFs) [19], gray-level co-occurrence probability (GLCP) [25], wavelet transforms [39], wavelet packets and wavelet frames [6], and Gabor filters [30] are the state-of-the-art texture extraction methods. Furthermore, the idea of fusing the textures extracted from different techniques has attracted wide attention recently. In a paper by Clausi [8], he presented

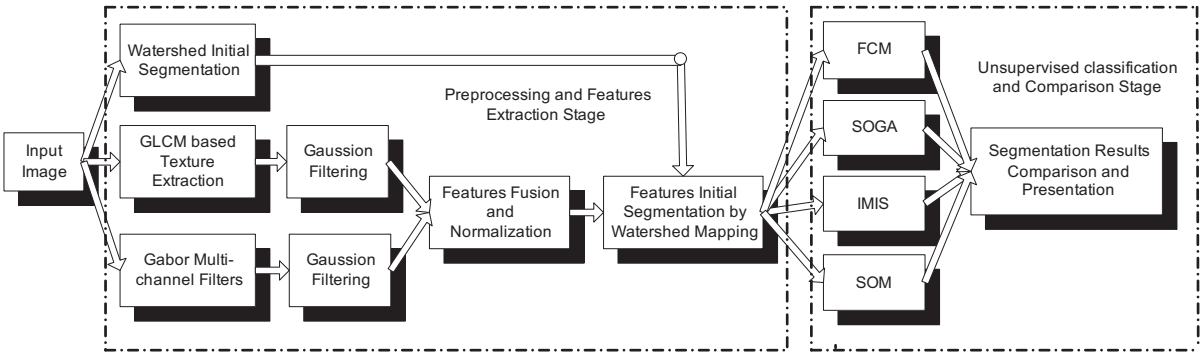

Fig. 1. The basic image segmentation framework using immune, multi-objective optimization, and three other classical algorithms.

the comparison and fusion of co-occurrence, Gabor, and MRF texture features to classify SAR imagery of sea ice. In this paper, above three techniques were compared in pairs and the fusion versions of them were investigated in analyzing textures of SAR images of sea ice. In another paper [40], Ruiz compared four different approaches of texture features extraction in remote sensing analysis, which were called GLCM, energy filters, Gabor filters, and wavelet transforms. They also assessed the potential performance of combinations of texture and spectral data from high-resolution satellite images. Besides, Solberg and Jain [42], they investigated the performance of texture features extracted by GLCP, local statistics, a fractal model, and a lognormal random field model. The discrimination abilities of these methods were compared and optimal combinations of the texture features were discussed. Importantly, Clausi et al presented a design-based texture feature fusion using Gabor-filters and GLCP [9]. Their classification performance of the fused features and individual ones are investigated respectively. It obtained the impressive experimental results for unsupervised texture classification when both of these methods are utilized. Appropriate combinations of features using different methodologies for pattern recognition could provide superior performance to individual ones. Therefore, Gabor filters and GLCP were both used for feature extraction because they can extract features at wider range of frequency components of SAR images.

3.1.2.1. Gabor filters. Gabor filters directly measure local frequency components by acting as a multi-channel, band-pass filter centered on the frequencies and orientations of interest. Clausi et al. have shown that Gabor filters are suitable for texture presentation and discrimination because they are mathematically tractable, simply implemented, and have optimal joint spatial-frequency resolution [10]. Gabor function is a Gaussian modulated complex sinusoid in the spatial domain. The 2-D Gabor function is defined by

$$g(x,y) = \frac{1}{2\pi\sigma_x\sigma_y}\exp\left[-\frac{1}{2}\left(\frac{x^2}{\sigma_x^2}+\frac{y^2}{\sigma_y^2}\right)+j2\pi F(x\cos\theta+y\sin\theta)\right] \tag{6}$$

where F is the modulation frequency and θ specifies the orientation of normal to the parallel stripes of the Gabor function. The raw filtering responses at different frequencies and orientations are features extracted by Gabor multi-channel filters. Commonly, Gaussian filters are employed for smoothing the raw Gabor magnitude response because they can generate the preferred segmentation results [10]. The Gaussian post filters have the same shape with the corresponding channel filters but with greater spatial extents, which is controlled by γ in $g(\gamma x, \gamma y)$. A γ of two-thirds is recommended by Bovik et al. [4].

3.1.2.2. GLCP. Gray-level co-occurrence texture measurements have been widely utilized in image texture analysis since they were proposed by Haralick et al. [25]. The GLCP is a joint probability matrix of how often two different combinations of pixel brightness values occur in a local window where these two pixels have a separation of a certain distance d and direction α. If an image is simply denoted by $I(x,y)$ with size of $N_x \times N_y$ and the levels of image gray is N_G, the items of GCLP matrix could be defined as follows:

$$P(i,j) = \frac{p(i,j/d,\alpha)}{\sum_{i,j}^{W} p(i,j/d,\alpha)} \tag{7}$$

where $p(i,j/d,\alpha)$ is the frequency of occurrence of gray levels i and j separated by distance d and direction α, and W is the total number of pixel pairs in the image window. Once the GLCP is calculated, several statistical parameters can be extracted from the GLCP. There are total 14 statistical parameters for the GLCP in the original paper [25], commonly, only three (contrast, entropy, and correction) are recommended for SAR image classification because of their ability to extract independent features and to create the preferred discrimination. The procedure of the preprocessing stage is shown in Table 1.

3.2. The immune Multi-objective framework for SAR imagery segmentation

In this section, the total AIS-based multi-objective image segmentation framework will be discussed. A flow chart of the framework is shown in Fig. 1. The framework consists of two stages: the stage of preprocessing and feature extraction, and the stage of unsupervised classification and comparison. The watershed initial segmentation in the first stage is a local and coarse classifier, which performs local pixels combination under the condition that the pixels in the same water basin are spatially contiguous. The immune, multi-objective, optimization algorithm (IMIS) in the second stage is a global fine classifier. The fused features of pixels are used for merging local patches produced by watershed transformation and there is no restriction on the spatial adjacency in the second stage. If the segmentation tasks have few categories and simple data distribution, it is possible for watershed transformation to solve the tasks perfectly in the first stage. Therefore, the superior performance of IMIS can only be demonstrated in segmenting image data with many numbers of true classes and complicated distribution. The inference will be validated in the following experiments.

In the previous work, we have performed profound research on the theories of AIS [31] and AIS-based, multi-objective optimization [22]. Based on the great deal of summarizations and comparisons in the current evolutionary, multi-objective optimization community, we believe that AIS-based, multi-objective algorithms have a superior selection pressure because of their use of the clonal selection principle and immune response operations, which can accelerate the evolutionary process in the population. Additionally, we have put forward an adaptive hybrid model, which utilizes the online discovered, non-dominated solutions to adaptively regulate the searching process [48,49]. In this study, we want to introduce an efficient and

Table 1
Algorithm 1: The stage of feature extraction and preprocessing.

Input parameters: Watershed transformation: input image I, dilation and erosion operations; Gabor filters: center frequencies F, orientations θ; GLCM: local window size w, inter-pixel distance δ, direction α, quantization level q
Output result: Raw segmentation results of fused features: *RSFeatures*
Step 1. Watershed raw segmentation
WI = *Watershed* (*I*); %*WI*: segment input image *I* by watershed transformation in Eq. (5)
maxWI = max(*WI*); % Build watershed mapping
for *I* = 0:*maxWI*
index = Find(*WI* == *i*);
IMapping = [*IMapping index*];% Add datum *index* to *IMapping*;
endfor
Step 2. Feature extraction and fusion using Gabor filters and GLCP
for each $f \in F$ ***do***
for each $th \in \theta$ ***do***
GF = *Gabor-filter*(*I*, *f*, *th*); %Gabor multi-channel filters using Eq. (6)
GF = *Gauss-filter*(*GF*, γ);
GaborFeature = [*GaborFeature GF*];
end for
end for
for each $al \in \alpha$ ***do***
GF = *GLCP*(*I*, *w*, δ, *q*, *al*);%Calculate the statistical parameters of the GLCP by Eq. (7)
GF = *Gauss-filter*(*GF*, γ);
GLCPFeature = [*GLCPFeature GF*];
end for
FusedFeatures = [*GaborFeature GLCPFeature*]; % Combine the *GaborFeatures* and the *GLCPFeatures*
FusedFeatures = *FusedFeatures* − *min*(*FusedFeatures*)/[*max*(*FusedFeatures*) − *min*(*FusedFeatures*)];
Step 3. Raw segmentation of fused features by mapping the results of watershed segmentation
for *i* = 1 to |*IMapping*|%|*IMapping*| denotes the cardinality of *IMapping*
index = *IMapping*(*i*);%Take out the *i*th item in *IMaping* created in **Step 1**
RSFeatures(*i*) = mean(*FusedFeatures*(*index*)); % Calculate the mean value of *FusedFeatures*(*index*)
end for

robust AIS-based, multi-objective optimization with adaptive rank clones and a diversity maintenance technique by *K*-nearest neighbor list. The adaptive ranks clones can select the online discovered solutions at different ranks to implement clone operator. The dynamic information of the online antibody population is efficiently exploited, and then proliferate them, which can introduce robustness and adaptability to the searching process in MO. Furthermore, the *K*-nearest neighbor list is established and maintained to update the solutions in the archive population for diversity maintaining. The *K*-nearest neighbors of each antibody are founded and stored in a list in memory. Once an antibody with a minimal product of *K*-nearest neighbors is deleted, the neighborhood relations of the remaining antibodies in the list in memory are updated. The ability of diversity maintaining of IMIS can be significantly improved compared with the crowding distance used in NNIA [22]. Another important feature of IMIS is the online discovered, non-dominated antibodies are selected to update the population. If there are lots of non-dominated antibodies in the current generation, few excellent antibodies located at less-crowded, Pareto-optimal front are selected for updating. Once there are few online discovered, non-dominated antibodies, the solutions in cloning pool is used to update population. The adaptive selection operator will be presented in **Step 6** in Table 2. Using these novel and adaptive strategies, we believe that the proposed method can perform stably and efficiently for multi-objective optimization. The procedure is described in Table 2.

4. Experimental study

4.1. Experimental setup

To study the performance of this framework, IMIS is tested on both synthetic texture images and real SAR images in this section. Besides, five other algorithms: FCM, SOGA [1], SOM [59], HMTseg [7], and SCE [55] are used to compare with the proposed algorithms. The source codes of the first three algorithms are programmed by the authors of the study in MATLAB 7.01 and SCE is provided by Dr. Zhang (xrzhang@mail.xidian.edu.cn) and the procedure of HMTseg can be downloaded from the website (http://www.dsp.rice.edu/software). All the experimentations are implemented on an HP Workstation xw9300 (2.19 GHZ, 16 GB RAM; Hewlett-Packard, Palo Alto, CA).

The optimal parameter settings are difficult to determine for Gabor filters and GLCP. Chang and Kuo [6] have noted that the most significant information in texture images usually appear in the intermediate frequency bands. Clausi have verified that the low- and middle-frequencies of texture information can be accurately acquired using Gabor multi-channel filters, and GLCP can provide stable texture discrimination ability in higher frequency components [9]. The parameters used in this study are as follows, considering the above propositions and conclusions. The Gabor multi-channel filters are created with six center frequencies (F = 6.1876, 4.3878, 3.9135, 3.6751, 3.3991, and 2.9551 pixels per cycle) and six orientations ($\theta = 0°$,

Table 2
Algorithm 2: The immune, multi-objective optimization for SAR imagery segmentation.

Input parameters: IMIS: input image I, number of clusters k, number of objectives K, number of iterations $Gmax$, population scale N, size clone pool c, crossover probability p_c and mutation probability p_m
Output result: Final segmentation result of image I:
Step 1. Call Algorithm 1: Get raw segmentation results of the fused features: $RSFeatures$
Step 2. Initialization
P_t = rand(N, $BoundariesOf\ RSFeatures$); %Generate the population randomly in the determined boundaries
Fit_t = FitnessCalculation(P_t); % Calculate the XB and JM indices by Eq. (2) and assign them to Fit_t
NA_t = FindNondominatedAntibodies(Fit_t, P_t); %Find the non-dominated antibodies using Eq. (4)
Set iteration point $t = 0$;
Step 3. Adaptive selection from different ranks
$i = 0$; rs = [ ]; PNN = [ ];
while $i < c$ ***do***
Find K nearest neighbors for each antibody in NA_t and denote them by NNi. Calculate their products of the K nearest neighbors for each item in NA_t and denote them by $PNNi$;
if $i + |NNi| < c$
$AC_t = [AC_t\ NA_t]$; %Add NA_t into AC_t;
else
$InsufficientNumber = c - i$;
Take the insufficient number in NA_t with smaller $PNNi$ and add them into AC_t
end if
$i = i + |NNi|$; rs = [rs i]; PNN = [PNN $PNNi$];
NA_t = FindNextBestNon-dominatedAntibodies (P_t);
end while
Step 4. Perform cloning on the selected c antibodies at different ranks:
for $i = 1$ to |rs|
rn = $N * rs/sum(rs)$;
for $j = 1$ to rs(i)
cn = rn(i) $*$ $PNNi$ /sum($PNNi$);% Take out $PNNi$ in PNN;
tempAC $= \underbrace{AC_t(i,j), AC_t(i,j), \ldots, AC_t(i,j)}_{cn(j)}$;
$C_t = [C_t$ tempAC];
end for
end for
Step 5. The affinity maturity operators:
C'_t = SBXCrossover(C_t, p_c); C''_t = PolynomialMutation(C'_t, p_m);
$NFit_t$ = FitnessCalculation(C''_t); % Calculate the indices in Eq. (2) and assign them to $NFit_t$
Step 6. The adaptive selection and diversity maintenance by K-nearest neighbors list:
$MAC_t = AC_t \cup C''_t$;
$NMAC_t$ = FindNondominatedAntibodies(MAC_t);%Find the non-dominated antibodies using Eq. (4)
Find K nearest neighbors for each antibody in $NMAC_t$ and denote it by NNi. Calculate their products of the K nearest neighbors for each item in $NMAC_t$ and denote them by $PNNi$
if $|NMAC_t| > N$
While $|NMAC_t| > N$
$NMAC_t$ = DeleteSolution($NMAC_t$, $PNNi$); %Remove the items in $NMAC_t$ with the minimal $PNNi$
$PNNi$ = Update($NMAC_t$, $PNNi$); % Update $PNNi$ for the remaining antibodies in $NMAC_t$
end while
else if $|NMAC_t| > c$ and $|NMAC_t| < N$
else if $|NMAC_t| \leqslant c$
end if
Step 7. Stop condition judgment: If $t > Gmax$ is satisfied, calculate $PBM\text{-}index$ of the antibodies in P_{t+1}, and export the antibodies with the maximum $PBM\text{-}index$ as the output of the algorithm; otherwise, $t = t + 1$, and go to **Step 3**

30°, 60°, 90°, 120°, and 150°). Furthermore, the parameters involved in designing the GLCP are the local window size w, the quantization level q, the inter-pixel distance δ, and the direction α. A 9×9 local window is adopted to estimate texture information for each pixel. A 64-level quantization, the inter-pixel distance $\delta = 1$, and the direction $\alpha = 0°$, 45°, 90°, and 135° are employed for feature representation. We can obtain 12-dimensional GLCP feature vectors by calculating the three statistics (contrast, entropy and correlation) from Eq. (7). In this study, total 48-dimensional feature vectors were used for subsequent segmentation, which were obtained from 36-dimensional feature vectors created by the Gabor filters and the 12-dimensional GLCP feature vectors.

How about the parameter settings of the six algorithms are? The specific experimental settings for them are presented in this paragraph for fair comparison. *Parameter settings in FCM*: the maximum number of iterations was 100 and the fuzzy exponent was 2.0. FCM was repeated five times in each run, and the best result was selected to reduce the instability in initialization. *Parameter settings in SOM*: the dimensions of the features map were 5×5. *Parameter settings in SCE*: the scaling parameter σ for each component of spectral clustering with the Nyström method (SC_Nys) was distributed randomly in the interval [1,10]. Two hundred feature vectors were sampled randomly from the features in SCE for each component of the SC_Nys. Thirty components of the SC_Nys were employed and combined for the final ensemble learning. *Parameter settings*

Table 3
Specific parameter settings in IMIS and SOGA.

Methods	Population size	Number of generations	Crossover probability	Mutation probability	Optimized index	Size of clone pool
IMIS	40	20	0.8	0.1	XB JM	20
SOGA	40	40	0.8	0.1	XB	–

in HMTseg: A Haar wavelet with three levels of decomposition was adopted for the wavelet transformation. The 64×64 image blocks were used for model training. The size of the raw HMT-based multi-scale classifications window was 8×8, 4×4, and 2×2 by the suggestion in the paper [7]. Parameter settings for IMIS and SOGA are presented in Table 3. Additionally, simulated binary crossover (SBX) and polynomial mutation operator were adopted many times in current EMOA literatures [11,22,48,49]. Here, we continue to use them for affinity maturity operation. For the stop criterion for IMIS and SOGA, the maximal number of function-evaluations for IMIS was 800 and 400 was set for SOGA because there are two optimization indexes in IMIS [18,22].

Which kinds of ways are used to assess the segmentation results? An intuitive way is to inspect the partitioning results with the eyes. Furthermore, more effective and convincing manner is to calculate the statistical results of the six algorithms over multiple runs. The statistical indices are divided into two categories: the internal and external ones. The internal indices are used to evaluate the goodness of partitions of data sets without true class labels. XB, JM, and PBM are representatives of the internal indices. The external indices require the true class labels, including accurate rate (AR), rand index [28], and adjusted rand index (ARI) [28]. Here, five indices are used to evaluate the performance of the final segmentation results, which are XB, JM, PBM, AR and ARI. The detailed definitions of AR and ARI can be found in [28], and three other indices have been presented in Section 2.

4.2. Analysis of experimental results

In this section, we will investigate the performance of the AIS-based, multi-objective optimization algorithm compared to five other pattern classification algorithms in segmenting three synthetic texture images and two real SAR images. The three synthetic texture images have two, four, and five categories from the Brodatz album of the University of Southern California.[1] In the following experiments, 30 independent runs on each test image were performed to evaluate and compare the robustness of the algorithms. The statistical results (mean and variance) of the selected metrics are shown in Tables 4 and 5. It is noteworthy that the real class labels of the three synthetic texture images are easily obtained; therefore, their segmentation results can be evaluated by the AR and ARI indices. However, the ground truth class labels of the SAR images are difficult to acquire. Thus, AR and ARI cannot be used to evaluate of the segmentation results of the two SAR images.

Figs. 2–4 show the segmentation results of the synthetic texture image with two, four, and five categories using FCM, SOGA, SOM, IMIS, HMTseg and SCE, respectively. Table 4 lists the statistical means and standard deviations of segmentation results over 30 independent runs. Fig. 2 shows that all six algorithms can obtain good segmentation results for the synthetic texture image with two categories. The reason may be that, once an effective and appropriate feature extraction technique is designed, the difficulty of classification task can be simplified enormously. Table 4 shows FCM and SOGA perform the best in segmenting the synthesized texture image, followed by IMIS. The statistical results of HMTseg and SCE are inferior to the

Table 4
The statistical means and standard deviations of the segmentation results of the three synthesized texture image over 30 independent runs.

Data set	Method	XB	JM	PBM	AR	ARI
Texture2	FCM	0.1261(0.0002)	297.6128(0.0021)	**1.9703**(0.0008)	**99.4098**(0.0011)	**0.9765**(0.0089)
	SOGA	0.1149(0.0002)	364.5140(0.0022)	1.5403(**0.0006**)	99.3998(0.0012)	0.9761(0.0001)
	SOM	0.1413(0.0001)	265.7456(0.0021)	1.4558(0.0008)	99.3607(0.0022)	0.9745(0.0001)
	IMIS	0.1406(0.0002)	280.3019(0.0022)	1.5529(0.0007)	99.3792(**0.0010**)	0.9754(**0.0000**)
	HMTseg	–	–	–	98.7793(0.2256)	0.9517(0.0088)
	SCE	–	–	–	98.7281(0.0024)	0.9498(0.0001)
Texture4	FCM	0.2924(0.0164)	111.9748(8.3792)	0.7136(0.0588)	86.4814(13.4882)	0.8755(0.1607)
	SOGA	0.2343(0.0132)	155.7982(9.5098)	0.7297(0.2604)	81.1752(14.8180)	0.8758(0.1701)
	SOM	0.4099(0.0140)	108.2735(8.4029)	0.4307(0.0823)	76.3222(12.2265)	0.7845(0.1337)
	IMIS	0.2443(0.0130)	125.8723(5.9111)	**0.8792**(**0.0111**)	**98.6142**(**0.0029**)	**0.9635**(**0.0001**)
	HMTseg	–	–	–	97.3498(0.0897)	0.9309(0.0023)
	SCE	–	–	–	96.8168(0.0098)	0.9178(0.0002)
Texture5	FCM	0.7209(0.4050)	98.2155(21.0367)	2.7655(0.4237)	84.8603(21.5286)	0.8956(0.0721)
	SOGA	0.1219(0.0172)	110.1688(9.6690)	2.6989(0.3892)	86.6389(6.3854)	0.8996(0.0571)
	SOM	0.1376(0.0278)	103.9490(1.4234)	2.3325(0.3741)	77.1517(3.0085)	0.7975(0.0144)
	IMIS	0.1991(0.0235)	102.1979(1.1285)	**3.0279**(**0.1347**)	**96.4925**(**2.1729**)	**0.9251**(**0.0208**)
	HMTseg	–	–	–	93.9183(0.6288)	0.8595(0.0111)
	SCE	–	–	–	92.7210(3.5862)	0.8484(0.0452)

Table 5
The statistical means and standard deviations of the segmentation results of the two SAR image over 30 independent runs.

Data set	Method	XB	JM	PBM
Real SAR1	FCM	0.3196(0.0112)	170.7836(0.1777)	0.8499(0.0042)
	SOGA	0.1669(0.0071)	175.1025(0.4184)	0.9040(0.0094)
	SOM	0.3042(0.0112)	141.2703(0.8591)	0.8267(**0.0211**)
	IMIS	0.2510(0.0062)	171.0940(0.1765)	**1.1348**(0.0024)
Real SAR2	FCM	0.4256(0.0757)	131.6360(4.7731)	0.4584(0.0959)
	SOGA	0.1983(0.0242)	162.4240(1.1779)	0.4237(0.0429)
	SOM	0.6445(0.3352)	118.1468(0.7821)	0.4326(0.0424)
	IMIS	0.2053(0.0784)	128.3862(0.3017)	**0.8499**(**0.0220**)

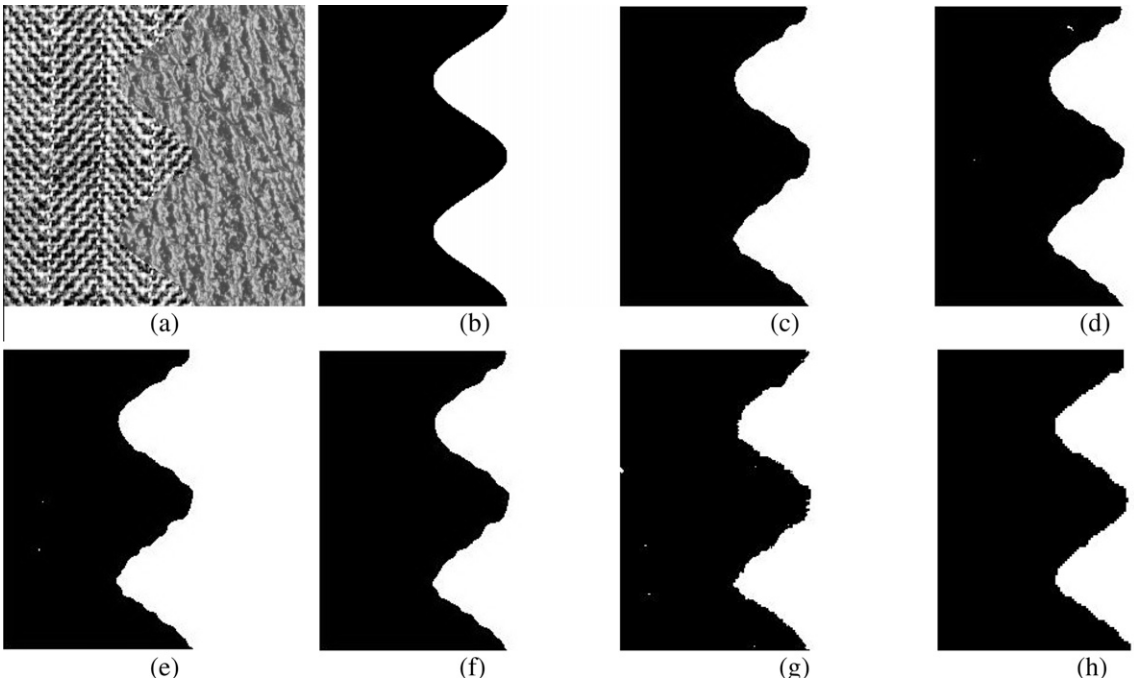

Fig. 2. The segmentation results of the synthesized texture image with two categories. (a) The original image (256 × 256 pixels); (b) The segmentation model and (c)–(h) the segmentation results by FCM, SOGA, SOM, IMIS, HMTSeg, and SCE, respectively.

other four algorithms in terms of AR and ARI indices. In order to further compare the six algorithms, more difficult classification tasks should be designed and tested. Once the true number of clusters is increased, the statistical results of the classification performance of the algorithms without global search ability will degrade.

In Fig. 3(d) and (e), some local patches are misclassified as other categories in the consistent regions. Thus, SOGA and SOM have demonstrated the relatively poor performance in segmenting the synthetic texture image with four categories. On the contrary, IMIS and HMTseg obtain the better segmentation results in region homogeneity, followed by SCE and FCM. Furthermore, the category boundaries in the middle of the partitioning results by HMTseg are not well divided. For SCE, there are two obviously misclassified spots at the lower right of its segmentation results. The statistical results in Table 4 also agree with the visually inspection in Fig. 3. SOGA aims to minimize the XB-index; thus, the optimal value of the index XB can be obtained by the algorithm. Nevertheless, it deteriorates greatly for another index, JM-index. The opposite case lies in FCM and SOM since both of them try to optimize the JM-index. Table 4 shows SOGA, FCM, and SOM cannot provide the best statistical values of PBM, AR, and ARI though they perform the best in optimizing XB-index or JM-index. For IMIS, the two indices are both incorporated in it and optimized simultaneously, the algorithm can obtained the best segmentation results both in visual inspection and statistical results of classification accuracy despite IMIS did not obtain the best in XB-index and JM-index. Therefore, we believe that the evolutionary process regulated by the two conflicting objectives is beneficial for searching the optimal partition, and the tradeoff solutions provided by them are useful for discovering the complicated relationships between image data.

Fig. 4 shows the segmentation results of the synthetic texture image with five categories using the six algorithms, respectively. Most of the real SAR images are contaminated by a lot of speckle noise, which could conceal and destroy regions or objectives of interest. It may cause difficulty and uncertainty for further discrimination and understanding. To simulate the

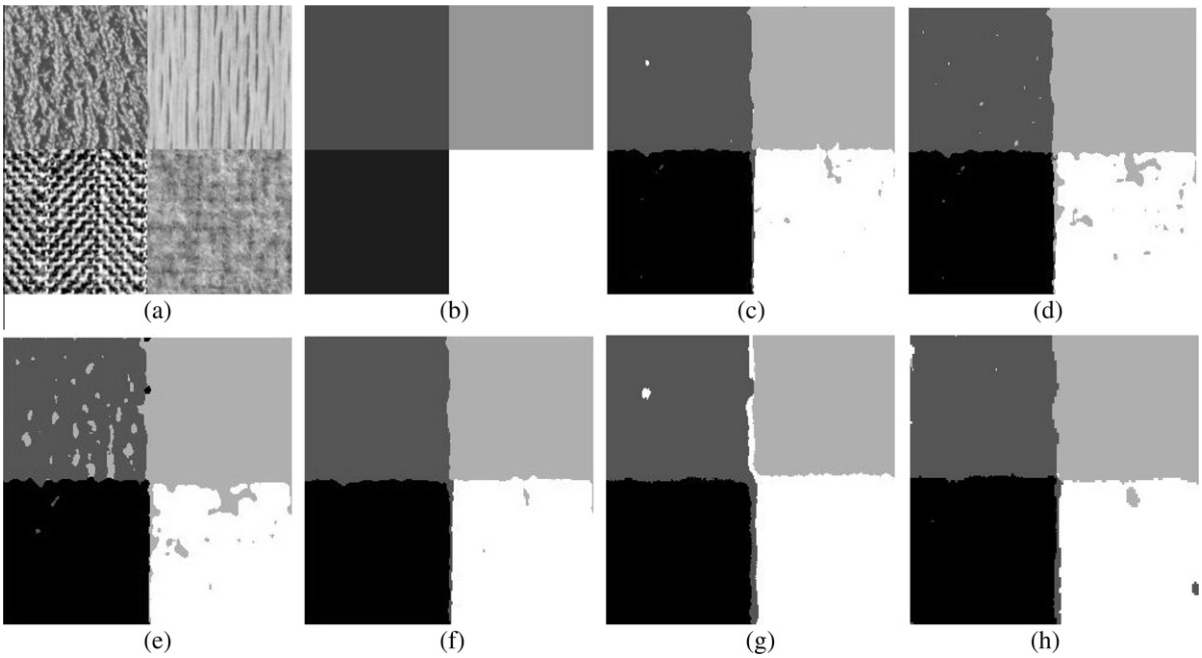

Fig. 3. The segmentation results of the synthesized texture image with four categories. (a) The original image (256 × 256 pixels); (b) the segmentation model and (c)–(h) the segmentation results using FCM, SOGA, SOM, IMIS, HMTSeg, and SCE, respectively.

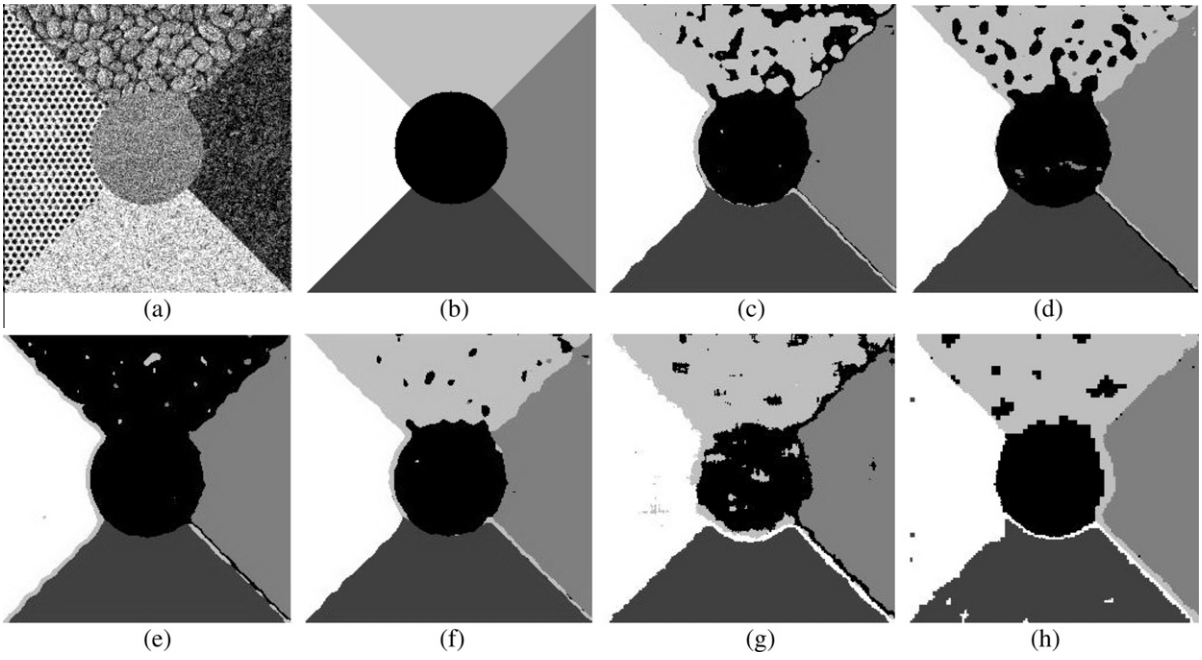

Fig. 4. The segmentation results of the synthesized texture image with five categories. (a) The original image (256 × 256 pixels); (b) the segmentation model and (c)–(h) the segmentation results using FCM, SOGA, SOM, IMIS, HMTSeg, and SCE, respectively.

effect of speckle noise on real SAR images, we added a high level of noise to the synthetic texture image with five categories. The added speckle noise has a mean of zero and a standard deviation of 35. Fig. 4 and Table 4 indicate IMIS is the best in visual inspection and statistical results of PBM, AR, and ARI. FCM and SOGA obtain the next-best one-off segmentation result in Fig. 4, but they show high instability over multiple runs in Table 4. To the best of the authors' knowledge, FCM is the widely used method for data clustering and image classification. The algorithm is easy to implement and gives reasonable

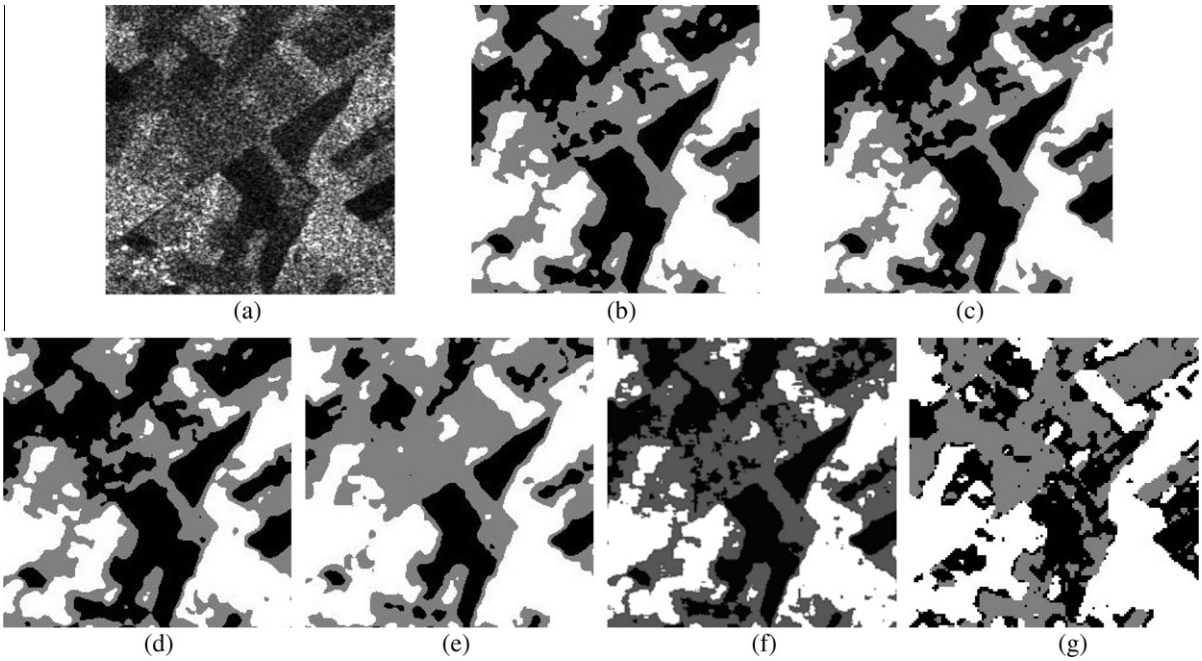

Fig. 5. The segmentation results of the SAR image with three categories. (a) The original image (256 × 256 pixels) and (b)–(g) the segmentation results using FCM, SOGA, SOM, IMIS, HMTSeg, and SCE, respectively.

results in most cases. Unfortunately, the algorithm makes local changes to the original partition. Thus, it often gets stuck at local minimum at the early iteration. Here, the segmentation results of the synthetic texture image with four and five categories have verified the conclusion. For SCE and HMTseg, the category boundaries of the segmentation results by them are not well defined. Considering the segmentation experimental results of six algorithms on the three synthesized texture images, we can conclude that IMIS has obtained impressive and encouraging partitioning results.

Additionally, in order to maintain the original intentions of the HMTseg and SCE algorithms, a multi-scale Haar wavelet is employed in HMTseg; gray-level co-occurrence matrix-based statistics and energy features from the undecimated wavelet decomposition are adopted in SCE. Therefore, the magnitudes of the features in HMTseg and SCE are different from the features in the other four algorithms in the framework. It is meaningless to compare their XB, JM, and PBM indices. Therefore, the three items of HMTseg and SCE in Table 4 are not presented.

The next two experiments were implemented using two real SAR images. Fig. 5 shows the segmentation results of a four-look SAR image provided by the second European Remote Sensing Satellite (ERS-2). The original image is shown in Fig. 5(a) and three types of crops in black, gray, and white. It can be seen that the gray crop in the middle of the image was seriously misclassified as black regions in Fig. 5(b), (c), and (d); whereas, the segmented results in Fig. 5(e) and (g) are better than the above three algorithms. The difficulty of segmenting the SAR image lies in the highly overlapping crops. Taking the regions at the upper right corner of the image as an example, the grayer crops and dark crops are mixed together. It can induce ambiguity for accurate and clear partitions. Similar regions are located at the upper middle, upper right, and middle right of the original image. Table 5 presents the statistical segmentation results of the SAR image over 30 independent runs. As seen in Fig. 5 and Table 5, IMIS and SCE have obtained more satisfying segmentation results than other four algorithms.

The last experiment was carried out on an SAR image of certain open field in the western China. The image consists of four typical ground objects: three types of crops and several regions of water. Visually, the difficulty of the classification task lies in how to distinguish the light gray crops, dark gray crops, and black water clearly and accurately. The segmentation results by FCM and SOM are shown in Fig. 6(b) and (d). They have same troubles in separating the light gray crops from the dark gray crops in the upper left corner of the image. Besides, some dark gray crops are misclassified as water regions. Fig. 6(c) shows the segmentation results by SOGA. Most of the light gray crops and the dark are mixed together, and we cannot find clearly partitioning results of the SAR images. For SCE, some dark gray crops are misclassified as light gray ones. In Fig. 6(e) and (f), IMIS and HMTseg have obtained the better partitions than FCM, SOGA, and SCE. In particular, IMIS seems presented relatively better results not only in region consistence but also in the boundary localization.

The statistical means and standard deviations of the segmentation results of the two SAR image over 30 independent runs are presented in Table 5. The statistical results of XB, JM, and PBM by HMTseg and SCE are not demonstrated in this study because the features used in HMTseg and SCE are different from the features in the other four algorithms. Table 5 shows that two complementary optimization indexes in IMIS could produce more suitable segmentation results despite that they are not at their optimal values.

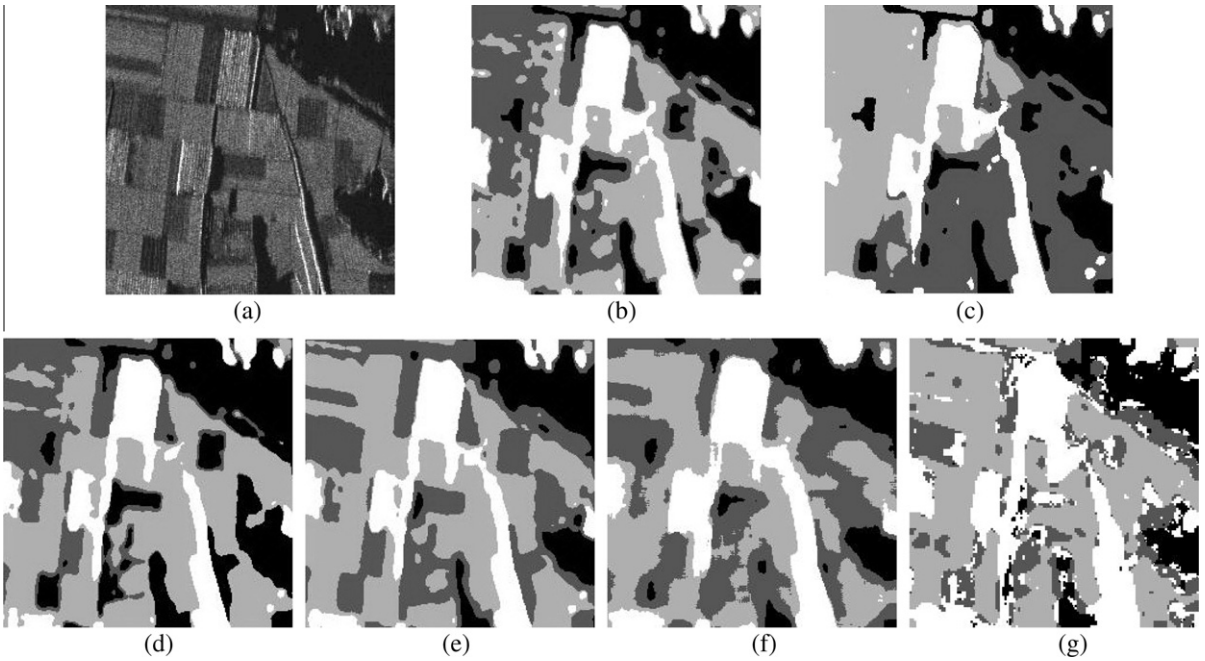

Fig. 6. The segmentation results of the SAR image with four categories. (a) The original image (256 × 256 pixels) and (b)–(g) the segmentation results by FCM, SOGA, SOM, IMIS, HMTSeg, and SCE, respectively.

4.3. Analysis of the involved parameters and key points in IMIS

4.3.1. The Effect of Watershed transformation on IMIS

How does the Watershed transformation contribute to the performance of the segmentation framework? The Watershed transformation is employed to preliminarily segment an image into many local non-overlapping patches. Table 6 shows the average running times, AR and ARI indices obtained by FCM, SOGA, SOM, and IMIS with or without Watershed transformation on the synthesized texture image with five categories. The average running times of IMIS with and without Watershed transformation are 10174.4521 (s) and 96.4472 (s), and their ratio is 105.4925, whereas the ratio of their accurate rates is 96.8469/96.4925 = 1.0041. We can see that the computational load is greatly reduced without a noticeable decline in clustering accuracy. Therefore, the Watershed transformation is a very practical and effective preprocessing strategy for segmenting images of large size.

4.3.2. The performance of IMIS with fused and individual features sets

It is necessary to study the performance of fused feature sets and individual feature set respectively since the fused features created by Gabor filters and GLCP are employed in this study. Table 7 shows the mean values of indices AI and ARI obtained by IMIS in segmenting the synthesized texture images with four and five categories over 30 independent runs. We can see the performance of IMIS with fused feature sets outperformed those of IMIS with non-fused feature sets. Therefore, we believe that fused feature sets possess both advantages of the Gabor filters and GLCP. Furthermore, the segmentation accuracies obtained by IMIS with Gabor filters are superior to these of IMIS with GLCP. The reason may be that the texture features are often prevalent in the middle-frequency bands, which can be captured by Gabor filters.

Table 6
The average running time and indices of AR and ARI obtained using FCM, SOGA, SOM, and IMIS with or without Watershed raw segmentation on the synthesized texture image with five categories.

Algorithms	Statistical results without Watershed			Statistical results with Watershed		
	Times (s)	AR (%)	ARI	Times (s)	AR (%)	ARI
FCM	77.9839	88.0078	0.8936	**3.4654**	84.8603	0.8956
SOGA	14652.2633	89.5688	0.8998	**150.2589**	86.6389	0.8996
SOM	969.8355	83.8281	0.8261	**61.3979**	77.1517	0.7975
IMIS	10174.4521	96.8469	0.9288	**96.4472**	96.4925	0.9251

Table 7
The statistical means and standard deviations of the segmentation results of the two synthesized texture images by IMIS with the features sets created by Gabor, GLCP, and Gabor + GLCP.

Data set	Method	AR	ARI
Texture4	IMIS with GLCP only	88.5775 (0.0876)	0.7252 (0.0017)
	IMIS with Gabor only	94.4016 (0.0733)	0.8609 (0.0016)
	IMIS with fused features	**98.6142** (**0.0029**)	**0.9635** (**0.0001**)
Texture5	IMIS with GLCP only	81.1308 (9.8594)	0.7581 (0.0529)
	IMIS with Gabor only	92.2562 (2.7319)	0.9051 (0.0345)
	IMIS with fused features	**96.4925** (**2.1729**)	**0.9251** (**0.0208**)

4.3.3. The sensitivity of IMIS to different levels of noise

We have investigated the sensitivity of IMIS to different levels of noise in this section. The mean values of the noise were zero and standard deviations of noise were in the range of [0, 200]. The noise was randomly created and the experimental results are presented by the average values of AR and ARI index over 30 independent runs. Fig. 7 shows the mean values of AR and ARI obtained by IMIS with fused features and Gabor features respectively in segmenting the synthesized texture image with five categories in presence of increasing noise. It can be seen that IMIS with fused features can obtain an accurate rate beyond 90% and an ARI greater than 0.9 when the standard deviation of noise is less than 50. Furthermore, the standard deviations of AR and ARI indexes are very smaller under this circumstance. Therefore, IMIS with fused features can perform very stable when the level of noise is less than 50. Its performance declines gradually when the standard deviation of noise is greater than 50. It can be expected that the critical noise level maybe have a standard deviation of 50 and a mean of zero. Furthermore, the segmentation accuracy of IMIS with Gabor features is inferior to that of IMIS with fused features. Therefore, the robustness and stability of Gabor features in representing and discriminating patterns in the presence of noise can be reinforced when GCLP features are combined.

4.3.4. The running time comparison and analysis

Table 8 shows the mean running times of FCM, SOGA, SOM, IMIS, HMTseg, and SCE in segmenting the synthesized texture image with five categories. In order to implement a fair comparison of the running time, the source codes of the six algorithms were implemented in Matlab 7.01 on an HP Workstation xw9300 (2.19 GHZ, 16 GB RAM; Hewlett-Packard, Palo Alto, CA). We can see that FCM is the least in computational times followed by SOM. However, they cannot obtain the best segmentation accuracy. As we know, IMIS, HMTseg, and SCE have performed better in partitioning above image data. It is unpleasant to accept the fact that they need a large amount of computational times. SCE requires the most running time in Table 8. The reason may be that ensemble operator merges many base-level classifiers by Nyström approximation. The main computational load of IMIS and SOGA lies in the population iterations and antibody selection. What is encouraging is that IMIS achieves the best segmentation results among the six algorithms. Additionally, it is interesting that the elapsed computational time of IMIS could be reduced greatly by Watershed transformation, and the segmentation accuracy almost

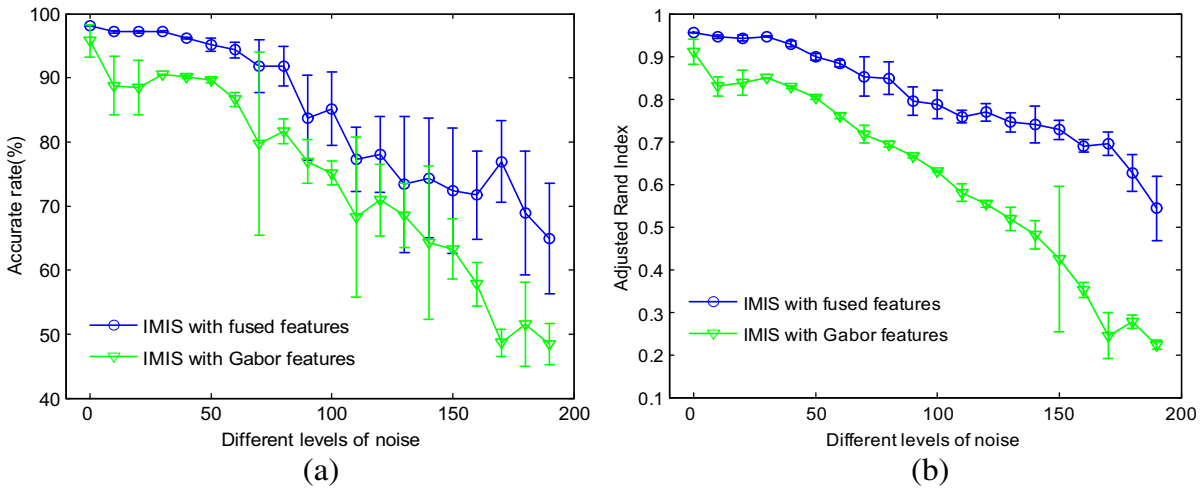

Fig. 7. The mean values of accurate rate (a) and adjusted rand index (b) obtained by IMIS with fused features and Gabor features in segmenting the synthesized texture image with five categories in the presence of increasing noise. The standard deviations of noise with a mean of zero increase from 0 to 200. The results are presented by error bar.

Table 8
The running times obtained using FCM, SOGA, SOM, IMIS, HMTseg, and SCE in segmenting the synthesized texture image with five categories.

Algorithms	FCM	SOGA	SOM	IMIS	HMTseg	SCE
Times (s)	3.4654	150.2589	61.3979	96.4472	113.5556	377.0743

remains the same. Therefore, it is possible to obtain a tradeoff between the computational time and the segmentation accuracy for practical image segmentation tasks.

5. Conclusion

To the best of our knowledge, most classical data clustering and image segmentation algorithms employ one internal clustering validity index to assess the goodness of partitions. The index is assumed to reflect the quality of the partitions. This assumption may be suitable for specific types of data sets, whereas it can not apply to different kinds of data sets equally. Here, an efficient, artificial immune, multi-objective image segmentation framework is proposed. Two conflicting indices are selected and optimized simultaneously in this framework. This AIS-based, multi-objective optimization algorithm was designed by incorporating an adaptive selection scheme, an adaptive rank clones and a diversity maintenance technique by dynamic *K*-nearest-neighbor list. The robustness, adaptability, and diversity maintenance of IMIS can be improved accordingly. Through the systematic experimental study in segmenting three synthetic texture images and two complicated SAR images, one can see good and encouraging partitioning results of IMIS has been obtained.

As we know, clustering validity indices play key roles in discovering the similarities and differences among data samples. Up to now, many indices have been proposed and some investigations on comparing their effectiveness in partitioning different types of pattern classification problems have been presented [37,46]. However, their combinatorial properties are seldom discussed. It is a possibility that although some individual index does not yield the best segmentation accuracy, their combinations in pairs or groups perhaps provide more suitable partitions.

Texture features extraction is another key technique in image segmentation, which deserves further study. Once suitable feature extraction techniques are proposed for certain classification tasks, the complexity of pattern discrimination can be greatly reduced. Currently, fused texture feature sets can produce the better segmentation results than individual feature set. However, fused texture sets may involve feature redundancy and the excessive computation time, which maybe degrade the performance of these classifiers [24]. Therefore, it is still a problem deserving further study to find efficient and suitable feature extraction methodologies for extracting different image features. The authors are currently working in this direction.

Acknowledgements

This work was supported by the National Natural Science Foundation of China (Grant Nos. 60703107, 60703108, 61001202), the National High Technology Research and Development Program (863 Program) of China (Grant No. 2009AA12Z210), the Program for New Century Excellent Talents in University (Grant No. NCET-08-0811), the Program for New Scientific and Technological Star of Shaanxi Province (Grant No. 2010KJXX-03), Beijing Municipal Natural Science Foundation (No. 7092020), and the Fundamental Research Funds for the Central Universities (Grant No. K50510020001).

References

[1] S. Bandyopadhyay, U. Maulik, A. Mukhopadhyay, Multi-objective genetic clustering for pixel classification in remote sensing imagery, IEEE Transactions on Geoscience and Remote Sensing 45 (5) (2007) 1506–1511.
[2] M. Bereta, T. Burczynski, Immune *K*-means and negative selection algorithms for data analysis, Information Sciences 179 (10) (2009) 1407–1425.
[3] F.J. Berlanga, A.J. Rivera, M.J. del-Jesus, F. Herrera, GP-COACH: genetic programming-based learning of compact and accurate fuzzy rule-based classification systems for high-dimensional problems, Information Sciences 180 (8) (2010) 1183–1200.
[4] A.C. Bovik, M. Clark, W.S. Geisler, Multi-channel texture analysis using localized spatial filters, IEEE Transactions on Pattern Analysis and Machine Intelligence 12 (1) (1990) 55–73.
[5] F.C. Chang, H.C. Huang, A refactoring method for cache-efficient swarm-intelligence algorithms, Information Sciences (2010) 11–12, doi:10.1016/j.ins.2010.02.025.
[6] T. Chang, C.J. Kuo, Texture analysis and classification with tree-structured wavelet transform, IEEE Transactions on Image Processing 2 (4) (1993) 429–441.
[7] H. Choi, R.G. Baraniuk, Multiscale image segmentation using wavelet-domain hidden Markov models, IEEE Transactions on Image Processing 10 (9) (2001) 1309–1321.
[8] D.A. Clausi, Comparison and fusion of co-occurrence, Gabor, and MRF texture features for classification of SAR sea ice imagery, Atmosphere – Oceans 39 (3) (2001) 183–194.
[9] D.A. Clausi, H. Deng, Design-based texture feature fusion using Gabor filters and co-occurrence probabilities, IEEE Transactions on Image Processing 14 (7) (2005) 925–936.
[10] D.A. Clausi, M.E. Jernigan, Designing Gabor filters for optimal texture separability, Pattern Recognition 33 (11) (2000) 1835–1849.
[11] C.A. Coello Coello, Evolutionary multi-objective optimization: a historical view of the field, IEEE Computational Intelligence Magazine 1 (1) (2006) 28–36.
[12] C.A. Coello Coello, N. Cruz Cortés, An approach to solve multi-objective optimization problems based on an artificial immune system, in: First International Conference on Artificial Immune Systems 2002, pp. 212–221.

[13] V. Cutello, G. Narzisi, G. Nicosia, A class of Pareto archived evolution strategy algorithms using immune inspired operators for ab-initio protein structure prediction, in: Applications on Evolutionary Computing, Evoworkshops 2005, Lausanne, Switzerland, Lecture Notes in Computer Science, vol. 3449, 2005, pp. 54–63.
[14] D. Dasgupta, S. Forrest, Novelty detection in time series data using ideas from immunology, in: Proceedings of the Fifth International Conference on Intelligent Systems, 1996, pp. 87–92.
[15] L.N. de-Castro, J. Timmis, Artificial Immune Systems: A New Computational Approach, L.N. Springer-Verlag, London, UK, 2002.
[16] P.A.D. de-Castro, F.J. Von Zuben, BAIS: a Bayesian artificial immune system for the effective handling of building blocks, Information Sciences 179 (10) (2009) 1426–1440.
[17] K. Deb, Multi-Objective Optimization using Evolutionary Algorithms, John Wiley & Sons, Chichester, UK, 2001, ISBN 0-471-87339-X.
[18] K. Deb, A. Pratap, S. Agarwal, T. Meyarivan, A fast and elitist multi-objective genetic algorithm: NSGA-II, IEEE Transactions on Evolutionary Computation 6 (2) (2002) 182–197.
[19] H. Deng, D.A. Clausi, Unsupervised image segmentation using a simple MRF model with a new implementation scheme, Pattern Recognition 37 (12) (2004) 2323–2335.
[20] Y. Dong, B.C. Forster, A.K. Milne, Comparison of radar image segmentation by Gaussian- and Gamma-Markov random field models, International Journal of Remote Sensing 24 (4) (2003) 711–722.
[21] F. Freschi, M. Repetto, VIS: an artificial immune network for multi-objective optimization, Engineering Optimization 38 (8) (2006) 975–996.
[22] M.G. Gong, L.C. Jiao, H.F. Du, L.F. Bo, Multi-objective immune algorithm with nondominated neighbor-based selection, Evolutionary Computation 16 (2) (2008) 225–255.
[23] M.G. Gong, L.C. Jiao, L.N. Zhang, Baldwinian learning in clonal selection algorithm for optimization, Information Sciences 180 (8) (2010) 1218–1236.
[24] S. Gunal, R. Edizkan, Subspace based feature selection for pattern recognition, Information Sciences 178 (19) (2008) 3716–3726.
[25] R.M. Haralick, K. Shanmugam, I. Dinstein, Textural features for images classification, IEEE Transactions on System, Man, and Cybernetics 3 (6) (1973) 610–621.
[26] H.C. Huang, Y.H. Chen, Genetic fingerprinting for copyright protection of multicast media, Soft Computing 13 (4) (2009) 383–391.
[27] W.L. Huang, L.C. Jiao, Artificial immune kernel clustering network for unsupervised image segmentation, Progress in Natural Science 18 (4) (2008) 455–461.
[28] L. Hubert, P. Arabie, Comparing partitions, Journal of Classification 2 (1) (1995) 193–218.
[29] A.K. Jain, R.P. Duin, J.C. Mao, Statistical pattern recognition: a review, IEEE Transactions on Pattern Analysis and Machine Intelligence 22 (1) (2000) 4–37.
[30] A.K. Jain, F. Farrokhnia, Unsupervised texture segmentation using Gabor filters, Pattern Recognition 24 (12) (1991) 167–186.
[31] L.C. Jiao, L. Wang, A novel genetic algorithm based on immunity, IEEE Transactions on Systems, Man and Cybernetics, Part A: Systems and Humans 30 (5) (2000) 552–561.
[32] S. Kukkonen, K. Deb, A fast and effective method for pruning of nondominated solutions in multi-objective problems, in: Proceedings of the 9th International Conference on Parallel Problem Solving from Nature (PPSN IX), Reykjavik, Iceland, 2006, pp. 553–562.
[33] C.H. Lee, O.R. Zaïane, H.H. Park, J.Y. Huang, R. Greiner, Clustering high dimensional data: a graph-based relaxed optimization approach, Information Sciences 178 (23) (2008) 4501–4511.
[34] C. Lemarechal, R. Fjortoft, P. Marthon, E. Cubero-Castan, A. Lopes, SAR image segmentation by morphological methods, in: Proceeding of the SPIE, vol. 3497, 1998, pp. 111–121.
[35] S.H. Leung, S.L. Wang, W.H. Lau, Lip image segmentation using fuzzy clustering incorporating an elliptic shape function, IEEE Transactions on Image Processing 13 (1) (2004) 51–62.
[36] G.C. Luh, C.H. Chueh, W.W. Liu, MOIA: multi-objective immune algorithm, Engineering Optimization 35 (2) (2003) 143–164.
[37] U. Maulik, S. Bandyopadhyay, Performance evaluation of some clustering algorithms and validity indices, IEEE Transactions on Pattern Analysis and Machine Intelligence 24 (12) (2002) 1650–1654.
[38] D.F. McCoy, V. Devarajan, Artificial immune systems and aerial image segmentation, in: International Conference on Computational Cybernetics and Simulation, vol. 1, 1997, pp. 867–872.
[39] T. Randen, J.H. Husy, Filtering for texture classification: a comparative study, IEEE Transactions on Pattern Analysis and Machine Intelligence 21 (4) (1999) 291–310.
[40] L. Ruiz, A. Fdez-Sarra, J. Recio, Texture feature extraction for classification of remote sensing data using wavelet decomposition: a comparative study, in: the 20th International Congress of Archives of Photogrammetry and Remote Sensing, Part B, 2004, pp. 1109–1115.
[41] J.D. Schaffer, Multiple-objective optimization with vector evaluated genetic algorithms, in: Genetic Algorithms and their Applications: Proceedings of the First International Conference on Genetic Algorithms, Lawrence Erlbaum, 1985, pp. 93–100.
[42] A.H. Schistad Solberg, A.K. Jain, Texture fusion and feature selection applied to SAR imagery, IEEE Transactions on Geoscience and Remote Sensing 35 (2) (1997) 475–479.
[43] J. Timmis, M. Neal, J. Hunt, Data analysis with artificial immune systems and cluster analysis and kohonen networks: some comparisons, in: Proceeding of the International Conference Systems and Man and Cybernetics, Tokyo, Japan, 1999, pp. 922–927.
[44] K. Trojanowski, S.T. Wierzchon, Immune-based algorithms for dynamic optimization, Information Sciences 179 (10) (2009) 1495–1515.
[45] L. Vincent, P. Soille, Watersheds in digital spaces: an efficient algorithm based on immersion simulations, IEEE Transactions on Pattern Analysis and Machine Intelligence 13 (6) (1991) 583–598.
[46] X.L. Xie, G. Beni, A validity measure for fuzzy clustering, IEEE Transactions on Pattern Analysis and Machine Intelligence 13 (8) (1991) 841–847.
[47] X. Yao, Y. Xu, Recent advances in evolutionary computation, Journal of Computer Science and Technology 21 (1) (2006).
[48] D.D. Yang, L. C Jiao, M.G. Gong, Adaptive multi-objective optimization based on nondominated solutions, Computational Intelligence 25 (2) (2009) 84–108.
[49] D.D. Yang, L.C. Jiao, M.G. Gong, J. Feng, Adaptive rank clone and k-nearest neighbour list based immune multi-objective optimization, Computational Intelligence 26 (4) (2010) 359–385.
[50] D.D. Yang, L.C. Jiao, M.G. Gong, X.Y. Si, J.J Li, and J. Feng, An effective immune multi-objective algorithm for SAR imagery segmentation, in: Proceedings of the SPIE, vol. 7494, 2009, doi:10.1117/12.832363.
[51] J. Yoo, P. Hajela, Immune network simulations in multicriterion design, Structural and Multidisciplinary Optimization 18 (2–3) (1999) 85–94.
[52] Q. Yuan, F. Qian, W.L. Du, A hybrid genetic algorithm with the Baldwin effect, Information Sciences 180 (5) (2010) 640–652.
[53] J. Zeng, W. Feng, L. Xie, Z.Q. Liu, Cascade Markov random fields for stroke extraction of Chinese characters, Information Sciences 180 (2) (2010) 301–311.
[54] L. Zhang, R.H. Li, Designing of classifiers based on immune principles and fuzzy rules, Information Sciences 178 (7) (2008) 1836–1847.
[55] X.R. Zhang, L.C. Jiao, F. Liu, L.F. Bo, M.G. Gong, Spectral clustering ensemble applied to texture features for SAR image segmentation, IEEE Transactions on Geoscience and Remote Sensing 46 (7) (2008) 2126–2136.
[56] X.R. Zhang, T. Shan, L.C. Jiao, SAR image classification based on immune clonal feature selection, Lecture Notes in Computer Science, vol. 3212, Springer, Berlin, 2004, pp. 504–511.
[57] L.P. Zhang, Y. F Zhong, B. Huang, J.Y. Gong, P.X. Li, Dimensionality reduction based on clonal selection for hyperspectral imagery, IEEE Transactions on Geoscience and Remote Sensing 45 (12) (2007) 4172–4186.
[58] H. Zheng, J.X. Zhang, S. Nahavandi, Learning to detect texture objects by artificial immune approaches, Future Generation Comput Systems 20 (7) (2004) 197–1208.

[59] Y.F. Zhong, L.P. Zhang, J.Y. Gong, P.X. Li, A supervised artificial immune classifier for remote-sensing imagery, IEEE Transactions on Geoscience and Remote Sensing 45 (12) (2007) 3957–3966.
[60] H.Y. Zhou, G. Schaefer, A.H. Sadka, M.E. Celebi, Anisotropic mean shift based fuzzy c-means segmentation of dermoscopy images, IEEE Transactions on Signal Processing 3 (1) (2009) 26–34.